Mapping of Io's Thermal Radiation by the Galileo Photopolarimeter-Radiometer (PPR) Instrument

J. A. Rathbun[1,2], J. R. Spencer[2], L. K. Tamppari[3], T. Z. Martin[3], L. Barnard[4], L. D. Travis[5]

E-mail: Julie_Rathbun@redlands.edu

[1]University of Redlands, 1200 East Colton Ave., Redlands CA 92373, USA
[2]Lowell Observatory, 1400 West Mars Hill Road, Flagstaff AZ 86001
[3]Jet Propulsion Laboratory, 4800 Oak Grove Drive, Pasadena CA 91109
[4]Raytheon Corporation, 299 S. Euclid Ave., Pasadena, CA 91109
[5]NASA-GISS, 2880 Broadway, New York, NY 10025

Manuscript pages: 39
Tables: 2
Figures: 7

Proposed Running Head: Galileo PPR at Io

Editorial correspondence to:

Dr. Julie A. Rathbun

Assistant Professor of Physics

1200 East Colton Avenue

PO Box 3080

Redlands, CA 92373-0999

Phone: 909-793-2121 ext 2927

Fax: 909-335-5121

E-mail: Julie_rathbun@redlands.edu

ABSTRACT

Between 1999 and 2002, the Galileo spacecraft made 6 close flybys of Io during which many observations of Io's thermal radiation were made with the Photopolarimeter-Radiometer (PPR). While the NIMS instrument could measure thermal emission from hot spots with T > 200 K, PPR was the only Galileo instrument capable of mapping the lower temperatures of older, cooling lava flows, and the passive background. We tabulate all data taken by PPR of Io during these flybys and describe some scientific highlights revealed by the data. The data include almost complete coverage of Io at better than 250 km resolution, with extensive regional coverage at higher resolutions. We found a modest poleward drop in nighttime background temperatures and evidence of thermal inertia variations across the surface. Comparison of high spatial resolution temperature measurements with observed daytime SO_2 gas pressures on Io provides evidence for local cold trapping of SO_2 frost on scales smaller than the 60 km resolution of the PPR data. We also calculated the power output from several hot spots and estimated total global heat flow to be about 2.0-2.6 W m^{-2}. The low-latitude diurnal temperature variations for the regions between obvious hot spots are well matched by a laterally-inhomogeneous thermal model with less than 1 W m^{-2} endogenic heat flow.

I. Introduction

Io, the closest Galilean satellite to Jupiter, is the most volcanically active body in the solar system. The Galileo spacecraft has been studying the Jupiter system since 1995 and between 1999 and 2002 made 6 close flybys of Io. Three remote sensing instruments are particularly useful in studying the active volcanism on Io: The solid-state imager (SSI), near-infrared mapping spectrometer (NIMS), and photopolarimeter-radiometer (PPR). Of these, PPR is the simplest (it is a single aperture photometer) and has the lowest spatial resolution (2.5 mrad) but, since it is sensitive from visible wavelengths up to 100 microns (Russell et al., 1992), it is the only instrument that can detect thermal radiation from surfaces colder than 200 K, such as low-temperature hotspots and the passive (sun-heated) surface between the hot spots. Here we describe all of the data taken by PPR at Io during the close flybys, and highlight some of the principle scientific results obtained from these data.

Though PPR can obtain visible-wavelength photometry and polarization data (Martin et al. 2000), at Io PPR was most often used in radiometry mode, in which the instrument operates in the thermal infrared. When it is the primary instrument, PPR usually builds up images by raster-scanning the Galileo scan platform across its target. When used in "ride-along" mode, in conjunction with another remote sensing instrument (either SSI or NIMS), PPR generally produces one-dimensional temperature scans. Three different filters were used for Io radiometry: a "17 µm" filter, covering the range 14.7 – 18.9 µm, used during some of the ride-along observations; a "27 µm" filter, covering the range 24.1 – 32.3 µm, usually used for dayside images; and an open filter, which is sensitive to radiation from the visible to 100 µm. The open filter is by far the

most sensitive filter for temperature mapping, but cannot be used for daytime observations because it cannot distinguish thermal radiation from reflected sunlight. It was thus normally used for nightside observations. Some nighttime observations included a flux contribution from reflected Jupiter light, which we estimate (Spencer et al 2000a) resulted in an overestimation of temperature of < 2 K. Observed flux in the discrete filters is most conveniently expressed as brightness temperature (T_B), which is the temperature of a blackbody emitting the observed flux at the observed wavelength. For the open filter, what we call brightness temperature is really effective temperature, defined as the temperature of a blackbody radiating the observed power at all wavelengths. Caution should be exercised in converting brightness temperatures to physical surface temperatures, especially for Io whose thermal emission spectrum deviates significantly from a blackbody (Spencer et al. 2003) due to both unresolved temperature contrasts within the field of view of most observations, resulting from local variations in albedo, thermal inertia, or volcanic heat, (McEwen et al. 1992, 1996), and spectral features due to non-unit emissivity which varies with wavelength due to spectrally-active surface species (Khanna et al. 1995). The flux is sampled and recorded at intervals of 0.46 seconds throughout an observation.

Radiation noise was a significant problem at Io, with noise levels several times higher than those seen at the orbits of Callisto or Ganymede, but could be reduced by averaging samples, and did not prevent useful observations. For example, one of our highest noise observations, the 27 µm observation 31IPDGTM_01 (Figure 1), has a noise of 26 DN in the unbinned data, corresponding to +/- 11 K at 120 K. Nyquist overlap of different fields of view, and subsequent smoothing of the image means that in this

5

particular observation each point on the surface is effectively observed about 50 times, giving 7-fold noise reduction to 1.6 K at 120 K. Nighttime data taken in the open filter has lower noise levels. For instance 31IPNSDRK_01 (Fig. 6) has a noise level of 6 DN before binning, corresponding to +/- 3K at 95 K. The scan rate for this observation covered the 2.5 mrad PPR field of view in 30 0.46 second samples, so binning by 15 samples, for Nyquist sampling, reduced the noise level to 1.5 DN, or 0.8 K.

Radiometric calibration of PPR data was checked using periodic observations of an on-board blackbody (the radiometric calibration target) of known temperature. PPR uses a chopper to rapidly compare observations of the sky with observations of the target, and drifts in internal temperature can sometimes produce spurious offsets of a few data numbers (DN) in the signal between the two beams. These offsets can be detected as non-zero DNs seen when looking at the sky off the limb of our targets.

Galileo orbits are generally described by a letter, which indicates the satellite Galileo flew closest to on that orbit, such as "I" for Io, followed by a number indicating the sequential number of that orbit. Excluding a close flyby of Io prior to Jupiter orbit insertion, when no remote sensing data were obtained, Galileo's Io flybys were I24, which took place October 10, 1999, I25 (November 25, 1999), I27 (February 22, 2000), I31 (August 5, 2001), I32 (October 15, 2002), and I33 (January 17, 2003). PPR was the only instrument to gather remote sensing data on I33, due to a spacecraft anomaly.

PPR data are archived in the form of a pair of ASCII data tables for each observation, giving the radiometric and geometric information for each 0.46 second sample. All data will shortly be available at the Planetary Data System Atmosphere

Node (http://atmos.nmsu.edu/atmos-home.html), and can also be obtained from http://www.lowell.edu/users/ppr/.

Brightness temperatures measured by PPR can be used in a variety of ways, some of which we begin to address in this paper. They can be used to study active volcanism and are particularly useful for measuring cooler lava flows near or below the ~ 200 K detection limit of NIMS (Carlson et al. 1992). From the flow's temperature, its age can be calculated from simple lava cooling models (e.g., Howell 1997). The total power from a volcanic hotspot can be calculated from its signal in the open filter when the hotspot is not resolved. Because the open filter detects all radiation emitted by Io, open filter observations are useful for estimating Io's total heat budget and endogenic heat flow. Passive surface temperature measurements constrain SO_2 frost temperatures, which are an important influence on atmospheric density and dynamics. The thermal inertia and other surface properties can be estimated from diurnal temperature variations.

II. Data

The PPR instrument obtained more than 100 observations of Io during the close flybys between 1999 and 2002 (Table I). Table I lists all PPR data of Io obtained in orbits I24 through I33. The observation name gives some information about the observation: the 2-digit orbit number is followed by the target (always "I" for Io in this case), the primary instrument (the instrument with primary control of the spacecraft pointing - "P" for PPR, "S" for SSI, and "N" for NIMS), and an 8-character name and number describing the observation. The table also gives the average resolution of the observation (which gives some indication of the extent of the observation), the average time of day (in degrees, defined as 0 at midnight, 90 at sunrise, and 180 at noon), the

7

average longitude and latitude, the total temperature range measured in the observation (large numbers indicate the presence of hotspots in the data), the duration of the observation, a description of the target, the time to closest approach (negative for before, positive for after) and the central wavelength of the filter used (in microns, with "O" indicating the open filter).

[Table I]

A. Data Reduction

Each PPR observation was corrected for internal temperature drifts by subtracting a fixed DN value from each sample that was equal to the DN measured when observing dark sky, either during that observation or during a nearby observation, so that sky level was zero in the corrected data. These corrections typically changed calculated brightness temperatures by less than 4 K. For raster scan data, we then created surface temperature maps with maximum possible resolution and S/N by projecting the PPR field of view onto the surface of the target for each sample time, and averaging the DNs in all overlapping fields of view at each location on the map. For 1-D scans we simply averaged DNs in overlapping fields of view along the scan direction. Finally, we converted the DNs to brightness temperatures, using algorithms developed during pre-launch calibration of PPR. Brightness temperature maps shown here are superposed on the appropriate portions of a global map of Io based on Galileo SSI images (McEwen et al. 1998a). Our experience is that PPR pointing accuracy is approximately 1 mrad compared to the 2.5 mrad instrument field of view, so only small corrections to the reported pointing are usually needed. Pointing is refined if necessary by reference to known volcanic features shown on the SSI-based base maps.

8

B. Daytime data

During I31, PPR obtained its first global daytime temperature map with good resolution (31IPDGTM__01, better then 300 km). For the most part, the 27 µm T_B distribution follows the expected pattern (Fig. 1) with T_B peaking near the subsolar point.

[Figure 1]

Hot spots are not obvious in this map, due to the relatively low resolution (300 km) and the relatively long wavelength. While some of the anomalously hot areas may be related to hotspots (Camaxtli at 16 N 137 W and Tupan at 18 S 141 W), other areas, such as 25 S 130 W are not associated with known hotspots or any obvious albedo feature. In the absence of volcanic hot spots, surface temperatures are controlled by the passive re-radiation of sunlight. Thermal inertia variations can have a significant effect on daytime temperatures on a relatively rapidly-rotating, cold object like Io (Spencer et al. 1989, Veeder et al. 1994) and may explain the non-volcanic anomalies (both high and low temperature) in the temperature distribution. On I27 we mapped a smaller area near the volcano Prometheus at 17 µm at somewhat higher resolution (Fig. 2), and saw similar local temperature patterns, though absolute brightness temperatures are higher than for the same region in Fig. 1 because the local time is closer to noon, and because T_B increases with decreasing wavelength (Spencer, 2003).

[Figure 2]

C. Nighttime data

Galileo obtained global nighttime temperature maps in the open filter during I27, I31, and I32; the I31 observation having the best resolution (223 km). Regional maps with higher resolution were made during I27, I31, and I32, giving near-complete

coverage of nightside temperatures at 200 – 100 km resolution. Figure 3 shows a
composite temperature map using the highest resolution available from all observations.
Galileo generally viewed only the Jupiter-facing hemisphere at night; so all maps include
only longitudes in the range 150 – 360 W. Due to the improved resolution over most
parts of this image, many hotspots can be seen, including some not previously detected
by Galileo. Hotspot names and locations are determined by identifying the Patera from
the USGS map that corresponds to the PPR hotspot .

[Figure 3]

Hotspots include: Loki, Amaterasu, Dazhbog, Daedalus, Babbar, Prometheus, Pele,
Marduk, Lei-Kung, Reiden, Kurdalagon, Svarog, and Ulgen (Table II). Two bright but
previously unknown north polar hot spots at 290 W, 76 N (corresponding to a prominent
dark spot in SSI images, now called Vivasvant Patera) and 245 W, 70 N (now called
Jumala Patera) were seen in the 31IPNPOLRG01 observation only, but may have been
present in other observations which had inadequate spatial resolution to resolve them.
There is a striking paucity of bright hot spots in the longitude range 160 – 200 W.

[Table II]

While most of the hotspots are clearly point sources even at regional scale
resolution, there are two notable exceptions: the enormous lava flows at Lei-Kung
Fluctus from 230 W, 55 N to 210 W, 45N, seen in I27, I31 and I32 global and northern
regional maps, and Lerna Regio, at 290 W, 60 S, seen in the 32IPBABBAR01 regional
map. Comparison of relatively low-resolution images from Voyager and Galileo implies
that both flows fields were emplaced before the Voyager encounter, and were therefore at
least 21 – 22 years old when observed by PPR. Both of these flows are located at high

10

latitude. Recent observations (Marchis et al. 2002, Howell et al. 2001, Lopes et al., 1999) have suggested that high-latitude eruptions on Io tend to be less frequent but larger than those at low latitudes, and the presence of these very large, still-warm lava flows at high latitudes is consistent with this pattern. Figure 4 shows a high resolution nighttime scan from I31 taken across Lei-Kung Fluctus. High temperatures correspond to the dark flows in the SSI basemap, as expected. Much of the southern part of the Lei-Kung flow has a nighttime temperature of 135 K, as warm as peak daytime passive temperatures, making it unlikely that the high nighttime temperature of Lei-Kung is due to an unusually high thermal inertia – such high nighttime temperatures almost certainly require an endogenic source. Also note that even at these mid-latitudes, background temperatures are 95 K, about the same as seen near the equator, suggesting little dropoff of temperature with latitude.

   [Figure 4]

Note that we cannot discount the possibility that the Lerna flow is warm at night due to high thermal inertia rather than release of endogenic heat, as peak nighttime temperatures at PPR resolution are only 103 K. Daytime observations of this flow, which PPR did not obtain, would be required to resolve the ambiguity. However Voyager IRIS observed Lerna Regio in daylight in 1979, and PPR/IRIS comparisons may provide clues to the nature of Lerna Regio.

   Nighttime passive temperatures are in the range 90 – 100 K, but with significant local variations. Temperatures are unusually low (near 86 K) in the inner ejecta blanket of Pele (#29), and in the ejecta from Babbar (#40). These are both unusual low-albedo deposits, where low temperatures might plausibly be due to low thermal inertias caused

by fine pyroclastic particles with poor grain-to-grain thermal conductivity (Wechsler et al. 1972). However, similar low temperatures are found in a region centered at 284 W, 25 S, which is a quite different-looking terrain of lava flows where a low thermal inertia may be less likely. There is also a well-defined high temperature (100 K) ring around Pele, about 5 K warmer than surrounding regions, which corresponds in position to the outer reddish-orange ring of Pele's plume deposits seen in visible wavelength images (McEwen et al., 1998a). This could be due to unusually high thermal inertia (caused, for instance, by sintering of particles in the ejecta blanket by condensing gas), or conceivably could result from surface heating by plume infall or condensation. Using the plume SO_2 column density measured by HST in October 1999 (7 x 10^{16} cm^{-2}, Spencer et al. 2000b), a plume ejection/impact speed of 1.1 km/sec (Spencer et al. 1997), a plume radius of 500 km, and an SO_2 latent heat of condensation of 24.92 kJ/mol (Dean 1992), we estimate that a 95.0 K surface would be heated to 95.25 K by the mechanical energy of impact of the SO_2 gas, and to 95.16 K by release of latent heat, if the SO_2 gas condensed on hitting the surface. These effects are too small to explain the observed 5 K temperature increase, but are not completely negligible. Mechanical heating could explain the anomaly if, for instance, the plume contained a dust mass much larger than the mass of gas. Arguing against plume heating as a cause of the warm ring is the fact that the plume is known to be highly variable (e.g. McEwen and Soderblom 1983, Spencer et al. 1997), but the magnitude of the thermal anomaly was similar during all three orbits (I27, I31, I32) in which Pele was mapped. Colchis Regio also shows large temperature variations that do not appear to be associated with low albedo regions (which normally suggest hotspots) and are likely to be due to thermal inertia variations.

Following the method of Spencer et al. (2000a), we can obtain a crude estimate of Io's global volcanic heat flow from these data by assuming that all nighttime emission above a model background temperature is volcanic. Following their method, we assume that passive nighttime temperatures have a $\cos^{1/4}$(latitude) dependence with a temperature of 95 K at the equator. In 31IPGLOBAL01, 38% of Io is covered, and we obtain a global mean heat flow of 2.6 W m^{-2} if we assume that the area covered by PPR is representative of the entire area of Io, or 2.0 W m^{-2} if we assume that Loki is unique and count its heat flow contribution only once. In the mosaic in Figure 3, 50% of the satellite is covered, and the global mean heat flow is calculated to be 2.4 W m^{-2} or 2.1 W m^{-2} if Loki is unique. Spencer et al. (2000a) found, using I25 and I27 PPR data which covered 45% of the surface, a heat flow of 2.0 W m^{-2} and 1.7 W m^{-2} if Loki is unique.

Figure 5 shows a high resolution scan from I27 taken across Loki Patera. The high temperatures correspond to the dark Loki caldera. Temperatures in the southwest corner of the patera are approximately 265 K, while those in the eastern portion are 285 K. This matches the lower-resolution I27 PPR Loki data presented in Spencer et al. (2000a) and Howell et al. (2001) and analyzed in Rathbun et al. (2002); as well as data presented in Marchis et al. (2001). This is a very different temperature distribution as that seen at Loki Patera during I24 (Spencer et al., 2000a; Rathbun et al., 2002). The data support the conclusions of Rathbun et al. (2002) that a resurfacing wave travels counter clockwise around Loki. Beyond the edge of the Patera, temperatures drop quickly, but not immediately, to 95 K. Based on comparison of data of this region at different resolutions, we believe that this slight rise in temperature, which extends for roughly six degrees beyond the edge of the caldera, is due to scattered light. Besides this ramp, the

13

background temperature shows very little spatial variability even at 15 km resolution, suggesting that unresolved small hot spots do not contribute significantly to this temperature, as it would be unlikely that the hot spot contribution would be similar in each 15 km field of view.

[Figure 5]

D. Diurnal and latitudinal temperature variations

Daytime temperatures on Io drop away from the subsolar point, as expected (Fig. 1). We also expect to see temperatures change as a function of the time of day and nighttime temperatures to drop at high latitudes. For surfaces in thermal equilibrium with instantaneous sunlight or diurnally-averaged sunlight, both night and day temperatures should vary as $\cos^{1/4}$(latitude), though intermediate thermal inertias can produce more complex latitudinal dependences . Following low-resolution nighttime maps from I27 which showed remarkably constant nighttime temperatures with latitude, during I31 PPR took high resolution (60 km) temperature scans from pole to pole during the day (31IPNSSTRP01) and from the equator to the southern pole at night (31IPNSDRK_01) to look more closely at latitudinal temperature variations. Figure 6 shows these scans, binned to the PPR field of view, along with the size and location of the fields of view.

[Figure 6]

Also shown are both scans on the same plot with $\cos^{1/4}$(latitude) curves for comparison. Note that hotspots contaminate the data. The daytime temperatures match the theoretical curve fairly well, except at high latitudes where data are less reliable. The nighttime temperatures exhibit a small but definite dropoff at high latitude, but much less than

14

expected from a $\cos^{1/4}$ law. The most likely explanation for the surprisingly warm

nighttime poles is that excess endogenic heat is being emitted from the polar regions.

Figure 7 shows equatorial background temperature as a function of time of day

from several observations. Again, the daytime temperatures from this diurnal

temperature curve match our expectations, with temperatures rising after sunrise (90) and

dropping after noon (180). Temperatures appear to drop during the night, but only

modestly (about 5 K). One possible explanation for the small temperature drop during

the night, along with the surprisingly small variation in nighttime temperature with

latitude, is that nighttime temperatures are *everywhere* dominated by endogenic heat and

that re-radiated sunlight is negligible on the night side, leading to a very high global heat

flow of up to 13.5 W (Matson et al. 2001).   However, given Io's known bolometric

albedo of about 0.52 (Simonelli et al. 2001), measurement of Io's total thermal radiation

shows that this heat flow is implausibly high (McEwen et al. 2003). That nighttime

temperatures between obvious hot spots are dominated by re-radiated sunlight can also be

seen from the thermophysical model fits (Spencer et al., 1989) to the diurnal curve shown

in Fig. 7, which use the Simonelli et al (2001) albedo of 0.52. A homogeneous surface

with a thermal inertia of 7×10^4 erg cm^{-2} s$^{-1/2}$ K matches the diurnal variation, but

laterally-inhomogeneous models with similar surface coverage of dark, low thermal

inertia and bright, high thermal inertia components provide a better match to the slow

nighttime cooling. A mixture of somewhat dark low thermal inertia pyroclastic dust and

bright, sintered, SO_2 frost would be one way to produce such a laterally inhomogeneous

surface, and similar inhomogeneous thermophysical models have been invoked

previously (Sinton and Kaminski 1989, Veeder et al. 1994). We also show an

inhomogeneous model in which background surface temperatures have been increased by an endogenic heat flow of 1 W m^{-2}, for instance by conduction through the crust or widespread low-temperature hot spots. It is clear that background equatorial heat flows much larger than 1 W m^{-2} would not be consistent with observed temperatures, given the known bolometric albedo, and that Io's observed heat flow of about 2 W m^{-2} is therefore dominated by the obvious large hot spots (which we avoided in Fig. 7), not by background heat flow.

[Figure 7]

Even the inhomogeneous thermophysical models in Fig. 7 predict greater nighttime cooling than is inferred from the observations. Perhaps the surface is even more inhomogeneous than the models, or perhaps the regions that PPR scanned early in the night have intrinsically lower nighttime temperatures (due to thermal inertia or albedo variations) than those scanned later in the night.

E. Frost Temperatures and Atmospheric Pressure

The daytime brightness temperatures can be compared to surface SO_2 frost temperatures inferred from the pressure of SO_2 in the atmosphere. Recent HST UV spectroscopy of the anti-Jovian hemisphere, centered on the Prometheus volcano, found peak SO_2 column densities for a low-latitude region near the subsolar point, centered at 8 N 162 W, of 2.5 x 10^{17} cm^{-2} (Jessup et al. 2003). If supported by vapor pressure equilibrium with surface frost, the inferred subsolar SO_2 frost temperature is near 119 K (Wagman 1979). However, 27 µm low-latitude subsolar temperatures (Figs. 6, 7) peak near 130 K, even in our highest resolution (60 km) observations which are the least likely to be contaminated by unresolved hotspots. Most likely, even the highest-resolution PPR

fields of view contain unresolved regions with varying passive temperatures. The SO_2

frost areal coverage is usually less than 100% at Galileo NIMS resolution (Douté et al

2001), and it is likely that the frost occupies cold traps, smaller than 60 km in extent,

within each PPR field of view. The cold frost temperatures are likely to be due to some

combination of high albedo and high effective thermal inertia (due for instance to grain

growth and sintering (Douté et al. 2001) or solid-state greenhouse effects (Matson and

Brown, 1989)), which will suppress daytime temperatures while enhancing nighttime

temperatures.

F. Hotspot power output

Many hotspots can be seen in the nighttime global and regional temperature maps

and most are unresolved. When they are unresolved, it is easy to calculate the total

power output from the hotspot by simply measuring the peak effective temperature of the

unresolved hotspot (T_p), the background temperature near the hotspot (T_a), and the area

of the projected PPR field of view (A), and assuming the surface radiates as a blackbody

with unit emissivity so that $P = \sigma A(T_p^4 - T_a^4)$, where σ is the Stefan-Boltzman constant.

Table II shows the calculated power output for the hotspots seen in maps from I25, I27,

I31, and I32. Errors in measuring the temperatures and areas of the hotspots lead to

variations of less than 0.05 W m^{-2}, however, if the entire hotspot does not lie in a single

field of view, we may be underestimating the power output by much more. Variations of

a single hotspot in images taken during the same orbit are likely to be due to errors. In

cases where the same hotspot was seen more than once, we also calculate the ratio

between the maximum and minimum power calculated, noted on the table as "Max/Min".

This should give us an idea of how changeable these hotspots are. The most dramatic

changes occurred at Dazhbog (303 W 55 N), where faint thermal emission was seen in I25, but it was dramatically brighter during I31 and I32, approaching the brightness of Loki, which is generally by far the brightest area on Io at these mid-infrared wavelengths (Spencer et al., 2000). This implies that the eruption of the pyroclastic deposits around Dazhbog seen by SSI during I31 was associated with extensive lava flows (McEwen et al., 2003). Pillan, where a major eruption was first observed in June 1997 (McEwen et al. 1998b) gradually decreased in flux, probably due to cooling of the 1997 lava flows. Loki also goes through significant changes, though since it is usually located near the limb and is often resolved, its power is more complicated to measure.

III. Conclusions

We have tablulated all of the data taken by PPR at Io during the 1999 – 2002 close encounters, and presented some scientific highlights from this rich data set. These data give a very detailed characterization of nightside temperatures with near-complete coverage at better than 200 km resolution. The better resolution nightside data show a modest poleward drop in background temperatures, though not as rapid as the expected $\cos^{1/4}$(latitude), perhaps indicating excess endogenic emission near the poles. Background temperatures at low latitudes, however, are dominated by re-radiated sunlight. The data show passive nighttime thermal anomalies in many places, notably in the Pele pyroclastic deposits. Many hotspots can be seen, their power output measured and compared at different times from different orbits. Large flux increases were seen at Dazhbog. Only two large, extended, hotspots were found, Lei-Kung Fluctus and Lerna Regio, which appear to be pre-Voyager lava flows.

Only one good (300 km resolution) global daytime temperature map was obtained (31IPDGTM__01). Unlike the nighttime temperatures, daytime temperatures vary strongly, and in the expected manner, with both latitude and local time. Comparison of high spatial resolution temperature measurements with observed daytime SO_2 gas pressures on Io provides evidence for local cold trapping of SO_2 frost on scales smaller than the 60 km resolution of the PPR data.

In this paper we have just begun analysis of this large and fascinating data set. We hope that our presentation of the data leads to more thorough analysis and more understanding of the processes at work on Io.

Acknowledgments

References

Carlson, R.W., P.R. Weissman, W. D. Smythe, J.C. Mahoney, and NIMS science and engineering teams 1992. Near infrared spectrometer experiment on Galileo. *Space Sci. Rev*. **60**, 457-502.

Dean, J. A. 1992. *Lange's Handbook of Chemistry,* 14th Edition, McGraw-Hill, New York.

Douté, S., B. Schmitt, R. Lopes-Gautier, R. Calson, L. Soderblom, J. Shirley, and the Galileo NIMS Team 2001. Mapping SO_2 Frost on Io by the Modeling of NIMS Hyperspectral Images. *Icarus* **149**, 107-132.

Howell, R. R. 1997. Thermal emission from lava flows on Io. *Icarus* **127**, 394-407.

Howell, R. R., J. R. Spencer, J. D. Goguen, F. Marchis, R. Prangé, T. Fusco, D. L.
Blaney, G. J. Veener, J. A. Rathbun, G. S. Orton, A. J. Grocholski, J. A.
Stansberry, G. S. Kanner, and E. K. Hege 2001. Ground-based observations of
volcanism on Io in 1999 and early 2000. *J. Geophys. Res*. **106**, 33129-33140.

Jessup, K.L., J.R. Spencer, G.E. Ballester, R.R. Howell, F. Roesler, M. Vigil, and R.
Yelle 2003. The Atmospheric Signature of Io's Prometheus Plume and Anti-
Jovian Hemisphere: Evidence for a Sublimation atmosphere. This issue.

Khanna, R.K., J.C. Pearl, and R. Dahmani, 1995. Infrared spectra and structure of solid
phases of sulfur trioxide: Possible identification of solid SO_3 on Io's surface.
Icarus **115**, 250-257.

Lopes-Gautier, R., A. S. McEwen, W. B. Smythe, P. E. Geissler, L. Kamp, A. G. Davies,
J. R. Spencer, L. Keszthelyi, R. Carlson, F. E. Leader, R. Mehlman, L. Soderblom
and the Galileo NIMS and SSI Teams 1999. Active Volcanism on Io: Global
Distribution and Variations in Activity. *Icarus* **140**, 243-262.

Marchis, F., R. Prangé, and T. Fusco 2001. A survey of Io's volcanism by adaptive optics
observations in the 3.9-μm thermal band (1996-1999). *J. Geophys. Res*. **106**,
33141-33160.

Marchis, F., I. de Pater, A. G. Davies, H. G. Roe, T. Fusco, D. Le Mignant, P. Descamps,
B. A. Macintosh, and R. Prangé 2002. High-Resolution Keck Adaptive Optics
Imaging of Violent Volcanic Activity on Io. *Icarus* **160**, 124-131.

Martin, T. Z., J. D. Goguen, L. D. Travis, L. K. Tamppari, L. Barnard, and L. Doose
2000. Galileo PPR polarimetric phase curves for the Galilean satellites. *Bull. Am.
Astron. Soc.* **32**, 39.4 (abstract).

Matson, D. L. and R. H. Brown 1989. Solid-state greenhouses and their implications for
icy satellites. *Icarus* **77**, 67-81.

Matson, D.L., T.V. Johnson, G.J. Veeder, D.L. Blaney, and A.G. Davies 2001. Upper
bound on Io's heat flow. *J. Geophys. Res*. **106**, 33021-33024.

McEwen, A. S. 1988. Global color and albedo variations on Io. *Icarus* **73**, 385-426.

McEwen, A.S. and L.A. Soderblom 1983. Two classes of volcanic plumes on Io. *Icarus*
55, 191-217.

McEwen AS, Isbell NR, Pearl JC. 1992. Io thermophysics: New models with Voyager 1
thermal IR spectra. *Lunar. Planet Sci*. **XXIII,** 881 (abstract).

McEwen, A.S., N.R. Isbell, K.E. Edwards, and J.C. Pearl 1996. Temperatures on Io:
Implications to geophysics, volcanology, and volatile transport. *Lunar Planet.
Sci.* **XXVII**, 843-844 (abstract).

McEwen, A. S., L. Keszthelyi, P. Geissler, D. P. Simonelli, M. H. Carr, T. V. Johnson, K.
P. Klaasen, H. H. Breneman, T. J. Jones, J. M. Kaufman, K. P. Magee, D. A.
Sensky, M. J. S. Belton, and G. Schubert 1998a. Active volcanism on Io as seen
by Galileo SSI. *Icarus* **135**, 181-219.

McEwen, A.S., L. Keszthelyi, J.R. Spencer, G. Schubert, D. L. Matson, R. Lopes-
Gautier, K.P. Klaasen, T.V. Johnson, J.W. Head, P. Geissler, S. Fagents, A.G.

Davies, M.H. Carr, H.H. Breneman, and M.J.S. Belton 1998b. High-temperature

silicate volcanism on Jupiter's moon Io. *Science* **281**, 87-90.

McEwen, A.S., L. Keszthelyi, R. Lopes, P. Schenk, and J. Spencer 2003. The lithosphere

and surface of Io.   In *Jupiter* (F. Bagenal Ed.) Cambridge University Press, in

press.

Rathbun, J. A., J. R. Spencer, A. G. Davies, R. R. Howell, and L. Wilson 2002. Loki, Io:

A periodic volcano. *Geophys. Res. Lett*. **29**, 10.1029/2002GL014747.

Russell, E. E., F. G. Brown, R. A. Chandos, W. C. Fincher, L. F. Kubel, A. A. Lacis, and

L. D. Travis 1992. Galileo Photopolarimeter/Radiometer experiment. *Space Sci.

Rev*. **60,** 531-563.

Simonelli, D.P., C. Dodd, and J. Veverka 2001. Regolith variations on Io: Implications

for bolometric albedos*. J. Geophys. Res*. **106**, 33241 -33252.

Sinton, W. M., and C. Kaminski 1988 Infrared observations of eclipses of Io, its

thermophysical parameters, and the thermal radiation of the Loki volcano and

environs. *Icarus* **75**, 207-232.

Spencer, J. R., L. A. Lebofsky, and M. V. Sykes 1989. Systematic biases in radiometric

diameter determinations. *Icarus* **78**, 337-354.

Spencer, J. R., P. Sartoretti, G. E. Ballester, A. S. McEwen, J. T. Clarke, and M. A.

McGrath 1997. Pele plume (Io): Observations with the Hubble Space Telescope.

Geophys. Res. Lett. **24**, 2471.

Spencer, J. R., J. A. Rathbun, L. D. Travis, L. K. Tamppari, L. Barnard, T. Z. Martin, and

A. S. McEwen 2000a. Io's thermal emission from the Galileo Photopolarimeter-

Radiometer. *Science* **288**, 1198-1201.

Spencer, J.R, K.L. Jessup, M.A. McGrath, G.E. Ballester, R. Yelle 2000b. Discovery of
Gaseous S_2 in Io's Pele Plume. *Science* **288**, 1208-1210.

Spencer, J. R., R. W. Carlson, and T. Becker 2003. Appendix: Maps and Spectra. In
Jupiter (F. Bagenal Ed.) Cambridge University Press, in press.

Wagman, D.D. 1979. Sublimation pressure and enthalpy of SO_2. Chem. Thermodyn.
Data Center, Natl. Bureau Standards, Washington, DC.

Wechsler, A. E., P. E. Glaser, A. D. Little, and J. A. Fountain 1972. Thermal properties
of granulated materials. In *Thermal Characteristics of the Moon*, J. W. Lucas,
Ed., MIT Press, Cambridge, pp 215-241.

Veeder, G. J. D. L. Matson, T. V. Johnson, D. L. Blaney, and J. D. Gougen 1994. Io's
heat flow from infrared radiometry: 1983-1993. *J. Geophys. Res*. **99**, 17095-
17162.

Table I

Galileo PPR observation of Io

Observation name	Res. (km)	Time of day	Lon.	Lat.	ΔT	Dura-tion	Target	Time to C/A	λ (μm)
24iploki__02	34	27	172	18	0	0:38:25	Loki	-0:50:37	17
24inpele__01	8	32	308	13	39	0:01:21	Pele	-0:04:06	17
24ispele__01	4	84	257	-18	69	0:00:46	Pele	-0:02:45	17
24ispillan01	2	99	242	-10	58	0:01:01	Pillan	-0:01:50	17
24inpillan01	2	100	241	-10	31	0:02:05	Pillan	-0:00:49	17
24iscolchs01	2	126	215	4	34	0:01:48	Colchis	0:01:17	17
24incolchs01	3	129	212	4	45	0:01:11	Colchis	0:03:05	17
24iszamama01	5	169	173	18	33	0:02:50	Zamama	0:04:17	17
24inzamama01	6	172	170	17	38	0:01:58	Zamama	0:07:08	17
24ispromth01	30	190	242	-10	0	0:06:17	Prometheus	0:09:07	17
24inpromth01	38	192	225	-13	0	0:02:44	Prometheus	0:15:25	17
24iscolchs02	21	130	213	5	4	0:01:17	Colchis	0:18:10	17
24incolchs02	23	129	214	3	7	0:02:07	Colchis	0:19:27	17
24istohil_01	23	182	162	-28	52	0:01:41	Tohil	0:21:35	17
24inntohil01	26	186	159	-26	0	0:03:10	Tohil	0:23:17	17
24ispromth02	30	190	155	-12	16	0:02:29	Prometheus	0:26:29	17
24inpromth02	38	192	154	-1	17	0:11:38	Prometheus	0:28:59	17
24iszamama02	48	152	195	25	64	0:04:34	Zamama	0:40:39	17
24inzamama02	52	175	172	18	2	0:03:49	Zamama	0:45:13	17
24isdorian01	55	171	177	-2	0	0:01:23	Dorian	0:49:07	17
24indorian01	57	163	186	-21	0	0:02:10	Dorian	0:50:31	17
24isamskgi01	62	242	107	21	67	0:04:34	Amirani	0:52:42	17
24inamskgi01	66	234	115	24	3	0:03:46	Amirani	0:57:17	17
24istermap01	71	260	90	1	0	0:01:41	Terminator	1:01:07	17
24intermap01	73	254	96	-5	0	0:02:01	Terminator	1:03:39	17
24inregion01	130	207	150	4	5	0:33:22		1:36:00	17
24inpplume01	161	135	225	-13	19	0:06:02		2:14:27	17
24inpelepm01	263	147	224	-18	6	0:06:04	Pele	3:33:17	17
24inregion02	529	201	194	8	28	0:17:11		6:10:01	17
24isglocol01	1645	221	235	7	0	0:03:02	Global	13:32:53	27
24iseclips01	3725	226	177	-2	0	0:09:06	Global	23:23:22	27
25ipglobal01	288	19	276	17	92	2:11:26	Global map	-5:14:56	O
25isemakng02	36	219	119	-4	21	0:07:13	Emakong	0:32:53	O
25inemakng02	39	221	117	-5	0	0:00:52	Emakong	0:37:44	O
25isgiants01					7	0:05:47	Tvashtar	0:40:58	O
25ingiants01	48	219	121	59	3	0:01:44	Tvashtar	0:43:31	O
25isculann01					15	0:07:29	Culann	0:47:02	O
25inculann01	54	181	159	-18	1	0:00:52	Culann	0:51:01	O
25isterm__01					8	0:04:59	Terminator	0:57:09	O
25intermap01	68	245	97	17	3	0:00:55	Terminator	1:01:34	O
25inregion01	86	197	147	6	8	0:54:36		1:04:14	O
27ipdrkmap01	344	22	240	-5	67	1:11:47	Global	-6:49:08	27
27iploki__01	116	350	308	9	156	1:00:40	loki	-2:27:15	O
27ipdaedal01	61	33	272	19	20	0:39:26	Daedalus	-1:21:32	O
27iploki__02	30	358	312	11	205	0:18:12	loki	-0:39:04	O
27iploki__03	15	1	311	12	198	0:08:05	Loki	-0:20:52	O
27inhrpele01	7	57	256	-18	29	0:07:05	Pele	-0:11:46	O
27ispele__01	4	59	255	-18	10	0:00:54	Pele	-0:05:28	O

Observation name	Res. (km)	Time of day	Lon.	Lat.	ΔT	Dura-tion	Target	Time to C/A	λ (μm)
27ispromth01	3	160	155	-1	146	0:02:01	Prometheus	0:04:11	17
27inmosaic01	18	160	157	13	12	0:14:02		0:11:23	17
27inpromth01	34	165	155	-2	17	0:10:07	Prometheus	0:30:42	17
27istohil_01	41	160	160	-28	14	0:01:27	Tohil	0:40:49	17
27ispromth02	42	167	154	2	21	0:02:35	Prometheus	0:42:16	17
27iscamaxt01	46	177	145	13	12	0:03:42	Camaxtli	0:44:51	17
27incamaxt01	49	186	136	14	13	0:02:00	Camaxtli	0:49:48	17
27isamrani01	52	207	115	23	14	0:01:34	Amirani	0:52:57	17
27inamrani01	60	208	115	27	15	0:18:40	Amirani	0:55:52	17
27iszaltrm01	84	253	73	35	56	0:03:55	Zal	1:19:14	17
27ipfrost_01	184	195	145	-8	21	1:11:47	Regional	2:24:57	17
27ipdgtm__01	256	204	144	47	43	2:00:19	Regional	3:34:43	27
31ipglobal01	223	335	237	8	59	1:41:07	Global	-4:43:19	O
31ippeledk01	145	332	252	-25	104	1:00:40	Pele	-3:02:12	O
31ipnpolrg01	99	333	257	62	53	0:55:06	Regional	-2:01:36	O
31ipnsdrk_01	56	348	249	-29	41	0:10:07	NS scan	-1:05:55	O
31iploki__01	40	291	308	13	152	0:10:07	Loki	-0:45:42	O
31ipleikng01	29	20	221	49	89	0:10:07	Lei-Kung	-0:35:35	O
31intherml01	14	347	256	-19	93	0:03:00		-0:32:33	O
31inhsisum01	7	38	206	33	91	0:06:04	Isum	-0:11:19	O
31iphires_01	2	4	240	55	121	0:05:03	Hi-res N. hem	-0:05:15	O
31inso2map01	3	145	101	70	1	0:06:04		0:02:50	O
31intvasht01	19	124	124	62	62	0:11:07	Tvashtar	0:14:58	O
31ingishbr01	40	162	89	17	8	0:16:09	Gish Bar	0:40:11	O
31ipnsstrp01	63	154	100	2	69	0:17:41	NS scan	0:57:22	27
31inamrani01	85	139	119	23	38	0:17:11	Amirani	1:20:41	27
31inregion01	143	138	206	33	0	0:34:23	Regional	1:51:01	27
31ipdgtm__01	298	149	138	-14	30	2:01:20	Global	4:03:29	27
32ipdrkmap01	639	331	194	5	18	0:31:21	Global	-11:04:25	O
32ipdrkmap02	331	323	246	8	30	1:07:45	Global	-6:08:10	O
32ipcolchs01	254	346	235	2	44	0:58:39	Colchis	-4:33:07	O
32ipregion01	193	333	257	33	57	0:59:39	Regional	-3:32:27	O
32ipbabbar01	132	313	286	-42	63	0:59:39	Babbar	-2:31:47	O
32iprapatr01	83	281	324	-9	38	0:29:19	Ra Patera	-1:31:07	O
32inthpele01	61	353	255	-18	71	0:05:03	Pele	-1:00:47	O
32iploki__01	44	305	305	14	190	0:19:13	Loki	-0:55:44	O
32inthloki01	23	303	311	11	85	0:11:07	Loki	-0:28:26	O
32ispele__01	17	353	262	-12	153	0:03:02	Pele	-0:17:19	O
32inthpele02	11	359	256	-17	48	0:07:05	Pele	-0:14:17	O
32iphiress01	3	334	287	-42	100	0:10:07	Hi-res S. hem.	-0:08:13	O
32istelgns01	1	120	135	-65	128	0:04:03		0:01:54	O
32intherml01	6	128	129	-78	6	0:04:03		0:05:57	O
32isemakng01	8	138	120	-23	84	0:01:27	Emakong	0:09:59	O
32istelgns02	9	140	118	-44	47	0:01:41	Telegonus	0:11:27	O
32istohil_01	14	100	159	-24	36	0:02:35	Tohil	0:13:08	O
32inemakng01	23	140	119	-4	38	0:11:07	Emakong	0:19:05	O
32istupan_01	35	117	145	-18	8	0:02:01	Tupan	0:33:15	O
32initupan01	40	120	141	-18	54	0:10:07	Tupan	0:35:16	O
32istvasht01	49	137	126	62	26	0:02:01	Tvashtar	0:45:23	O
32inichaac01	54	115	148	12	11	0:10:07	Chaac	0:47:24	O
32isgshbar01	61	167	97	16	2	0:02:21	Gish Bar	0:57:31	O
32inpromth01	72	133	133	41	12	0:13:09	Prometheus	1:01:33	O
32istermin01	81	103	164	-18	6	0:02:48	Terminator	1:14:42	O
32istermin02	83	116	152	34	14	0:02:08	Terminator	1:17:30	O

Observation name	Res. (km)	Time of day	Lon.	Lat.	ΔT	Dura-tion	Target	Time to C/A	λ (μm)
32ipewscan01	95	134	132	-1	74	0:14:09	EW scan	1:21:47	27
32ippolday01	212	136	146	47	31	0:30:20	Regional	2:53:47	27
33ipdrkmap01	1992	329	108	0	0	0:13:09	Global	-9:11:06	O
33ippromth01	66	38	156	-2	6	0:20:13	Prometheus	-1:04:50	O
33ipewscan01	45	21	175	0	3	0:05:03	Equator scan	-0:39:34	O
33ipmarduk01	35	350	210	-28	30	0:10:07	Marduk	-0:34:30	O

Table II

Hotspots and power output detected by PPR. NI indicates that the hotspot was not completely in the field imaged, ND indicates that the hotspot was not detected, R indicates that the hotspot was resolved and the power could not be measured with our method, and Sat indicates that the hotspot saturated the detector. If a hotspot was detected more than once, the radio between the highest and lowest power output is given as "Max/Min". The second column gives the # corresponding to the locations of hotspots shown on Figure 3. The second row indicates the observation: 25 is for 25ipglobal01 taken on 11/25/1999 at 22:50:04; 27a is for 27ipdrkmap01 taken on 2/22/2000 at 6:56:52; 27b is for 27iploki__01 taken on 2/22/2000 at 11:18:45; 31a is for 31ipglobal01 taken on 8/6/2001 at 12:15:41; 31b is for 31ippeledk01 taken on 8/6/2001 at 1:56:48; 31c is for 31ipnpolrg01 taken on 8/6/2001 at 2:57:24; 32a is for 32ipdrkmap02 taken on 10/15/2001 at 19:13:50; 32b is for 32ipcolchs01 taken on 10/15/2001 at 20:48:53; 32c is for 32ipregion taken on 10/15/2001 at 21:49:33; 32d is for 32ipbabbar01 taken on 10/15/2001 at 23:49:52; and 32e is for 32iprapatr01 taken on 10/15/2001 at 23:50:53.

Power Output (10^{12} W)													
Name of hotspot	#	25	27a	27b	31a	31b	31c	32a	32b	32c	32d	32e	Max/Min
Vivasvant	1	ND	ND	NI	NI	NI	0.27	NI	NI	NI	NI	NI	
Jumala	2	ND	ND	NI	ND	NI	0.24	0.4	NI	NI	NI	NI	1.67
Dazhbog	3	0.64	ND	NI	3.59	NI	Sat	4.38	NI	4.24	NI	NI	6.84
Unnamed, 264W, 53N	4	ND	ND	NI	ND	NI	0.15	ND	NI	0.04	NI	NI	3.75
North Lei-Kung	5	ND	ND	NI	ND	NI	R	0.45	NI	ND	NI	NI	
Amaterasu	6	0.92	0.91	NI	0.91	NI	NI	0.88	NI	NI	NI	NI	1.05
Atar	7	ND	ND	NI	ND	NI	NI	ND	NI	0.13	NI	NI	
Unnamed, 261W, 37N	8	ND	ND	NI	0.11	NI	NI	ND	NI	0.08	NI	NI	1.38

		Power Output (10^{12} W)											
Name of hotspot	#	25	27a	27b	31a	31b	31c	32a	32b	32c	32d	32e	Max/Min
South Lei-Kung	9	ND	ND	NI	ND	NI	NI	0.45	NI	R	NI	NI	1.25
Isum	10	ND	ND	NI	0.44	NI	NI	ND	NI	NI	NI	NI	
Mulungu + Susannoo	11	0.23	0.40	NI	0.43	NI	NI	0.42	R	NI	NI	NI	1.87
Girru	12	ND	ND	NI	0.11	NI	NI	0.19	0.16	0.14	NI	NI	1.73
Llew	13	ND	ND	NI	0.15	NI	NI	0.18	0.17	0.12	NI	NI	1.5
Shakuru	14	ND	ND	0.08	ND	NI	NI	ND	NI	ND	NI	NI	
Daedalus	15	R	R	R	1.79	NI	NI	1.43	NI	1.07	NI	NI	1.67
Fuchi	16	ND	NI	NI	NI	NI	NI	NI	NI	NI	NI	NI	
Acala	17	ND	NI	0.19	NI	NI	NI	NI	NI	NI	NI	NI	
Tol-Ava	18	ND	ND	0.08	NI	NI	NI	NI	NI	NI	NI	NI	
Loki	19	9.9	17.5	R	15.2	NI	NI	NI	NI	NI	NI	NI	1.77
Hephaestus	20	ND	ND	0.08	0.40	NI	NI	0.39	NI	NI	NI	NI	5
Tiermes	21	NI	NI	NI	NI	NI	NI	NI	NI	NI	NI	NI	
Ra	22	0.29	ND	NI	NI	NI	NI	NI	NI	NI	NI	0.06	
Mazda Catena	23	ND	ND	NI	NI	NI	NI	NI	NI	NI	NI	NI	
Huo Shen	24	ND	ND	NI	NI	NI	NI	NI	NI	NI	NI	NI	
Mihir	25	ND	ND	NI	ND	NI	NI	ND	NI	NI	0.18	NI	
Gibil	26	ND	ND	NI	ND	NI	NI	ND	NI	NI	0.13	NI	
Unnamed, 277W, 7S	27	ND	ND	NI	ND	0.05	NI	ND	NI	NI	NI	NI	
Unnamed, 278W, 13S	28	ND	ND	NI	ND	0.03	NI	ND	NI	NI	NI	NI	
Pele	29	NI	0.29	NI	0.27	0.25	NI	0.28	0.35	NI	NI	NI	1.4
Pillan	30	NI	2.55	NI	2.54	2.17	NI	1.48	1.55	NI	NI	NI	1.72
Unnamed, 233W, 4S	31	ND	ND	NI	ND	0.04	NI	ND	ND	NI	NI	NI	
Reiden	32	NI	ND	NI	ND	1.85	NI	ND	NI	NI	NI	NI	
Ot	33	ND	ND	NI	0.59	NI	NI	0.18	0.13	NI	NI	NI	4.54
Unnamed, 233W, 28S	34	NI	ND	NI	ND	0.04	NI	ND	NI	NI	NI	NI	
Unnamed, 224W, 24S	35	NI	ND	NI	ND	0.04	NI	ND	NI	NI	NI	NI	
Marduk	36	NI	0.84	NI	0.46	NI	NI	0.65	NI	NI	NI	NI	1.83
Wayland	37	NI	ND	NI	ND	0.05	NI	ND	NI	NI	NI	NI	
Kurdalagon	38	NI	0.44	NI	0.23	0.15	NI	ND	NI	NI	NI	NI	2.93
Unnamed, 236W, 49S	39	NI	ND	NI	ND	0.12	NI	ND	NI	NI	NI	NI	

		Power Output (10^{12} W)											
Name of hotspot	#	25	27a	27b	31a	31b	31c	32a	32b	32c	32d	32e	Max/Min
Babbar	40	NI	0.47	NI	0.33	0.50	NI	0.48	NI	NI	0.40	NI	1.52
Svarog	41	NI	ND	NI	ND	0.2	NI	ND	NI	NI	0.14	NI	1.43
Mithra	42	NI	ND	NI	ND	ND	NI	ND	NI	NI	0.08	NI	
Ulgen	43	NI	NI	NI	0.68	0.34	NI	0.88	NI	NI	0.73	NI	2.59
Sengen	44	NI	NI	NI	NI	NI	NI	NI	NI	NI	0.16	NI	
Rarog	45	NI	ND	NI	NI	NI	NI	NI	NI	NI	0.12	NI	
Aten	46	NI	NI	NI	NI	NI	NI	NI	NI	NI	ND	NI	
Heno	47	NI	ND	NI	NI	NI	NI	NI	NI	NI	0.25	NI	
Lerna	48	NI	ND	NI	NI	NI	NI	NI	NI	NI	R	NI	
Argos	49	NI	ND	NI	NI	NI	NI	NI	NI	NI	NI	NI	
Rata	50	NI	ND	NI	ND	NI	NI	NI	NI	NI	NI	NI	
Gabija	51	NI	ND	NI	ND	ND	NI	NI	NI	NI	NI	NI	
Unnamed, 206W, 55S	52	NI	ND	NI	ND	ND	NI	NI	NI	NI	NI	NI	

FIGURE CAPTIONS

Figure 1. Map of daytime brightness temperature in the PPR 27 micron filter, superimposed on an SSI map of Io, from the 31IPDGTM__01 observation. Contour interval is 5 K. Approximate location of the subsolar point is marked with an *.

Figure 2. Daytime equatorial brightness temperatures near the Prometheus volcano in the PPR 17 µm filter, from the 27IPFROST_01 observation. Contour interval is 2.5 K. Brightness temperatures may be higher than passive surface kinetic temperatures due to the relatively short wavelength of the observation, as discussed in the text.

Figure 3. Map of nighttime effective temperature in PPR's open filter, superimposed on an SSI map of Io. The temperature map is a composite of the highest-resolution global and regional observations from orbits I25, I27, I31 and I32, and shows artifacts at the boundaries between observations. Hot spots observed near Io's limb are elongated perpendicular to the limb when projected onto the map. Contour interval is 2.5 K, and contours above 130 K are omitted to avoid hiding the sources of the brightest hot spots. Hotspots are labeled with numbers that correspond to those listed in Table II. The map includes data from 25IPGLOBAL01; 27IPLOKI__01; 31IPNPOLRG; 31IPPELEDK01; 32IPBABBAR01; 32IPCOLCHS01; 32IPRAPATR01; AND 32IPREGION01.

Figure 4. Nighttime temperature scan across Lei-Kung Fluctus, in the open filter. The top two plots show effective temperature as a function of longitude while the bottom plot

shows the location and size of the PPR fields of view overlaid on an SSI image mosaic.

Data from 31IPLEIKNG01.

Figure 5. Nighttime temperature scan across Loki Patera. The top two plots show

brightness temperature as a function of longitude while the bottom plot shows the

location and size of the PPR fields of view overlaid on an SSI image mosaic. Data from

27IPLOKI__03.

Figure 6. Temperature variation with latitude. Temperature scans across Io taken during

the day (31IPNSSTRP01, left) and at night (31IPNSDRK_01, lower right). Next to the

scans are plots which show the location and size of the PPR fields of view overlaid on an

SSI image mosaic. The plot in the upper right shows both temperature scans and $\cos^{1/4}$

functions to compare the temperature drop at high latitudes with the expected drop.

Figure 7. Diurnal temperature variations. Measurements of temperature as a function of

time of day taken from several observations are plotted together. Time of day is given as

an angle, with 0 at midnight, 90 at sunrise, and 180 at noon. All data are averages taken

within 20 degrees of the equator and we have avoided obvious hotspots. The

32IPEWSCAN curve is an exception, as these are not data averaged from a map, but are

from a single scan across Io, binned to the PPR field of view. A hotspot (Prometheus at

local time 110°) can clearly be seen in this scan.   The smooth curves show thermal

models matched to the diurnal temperature variations. All have a mean albedo of 0.52,

consistent with Io's mean albedo. The homogeneous model has a thermal inertia of 7 x

10^4 erg cm^{-2} s$^{-1/2}$ K, while the inhomogeneous models have two surface components with equal areal coverage, one with albedo 0.34 and thermal inertia 4 x 10^4, and the other with albedo 0.70 and thermal inertia 1 x 10^6. The warmer inhomogeneous model includes an endogenic heat flow of 1 W m^{-2}, roughly the maximum background heat flow consistent with the data.
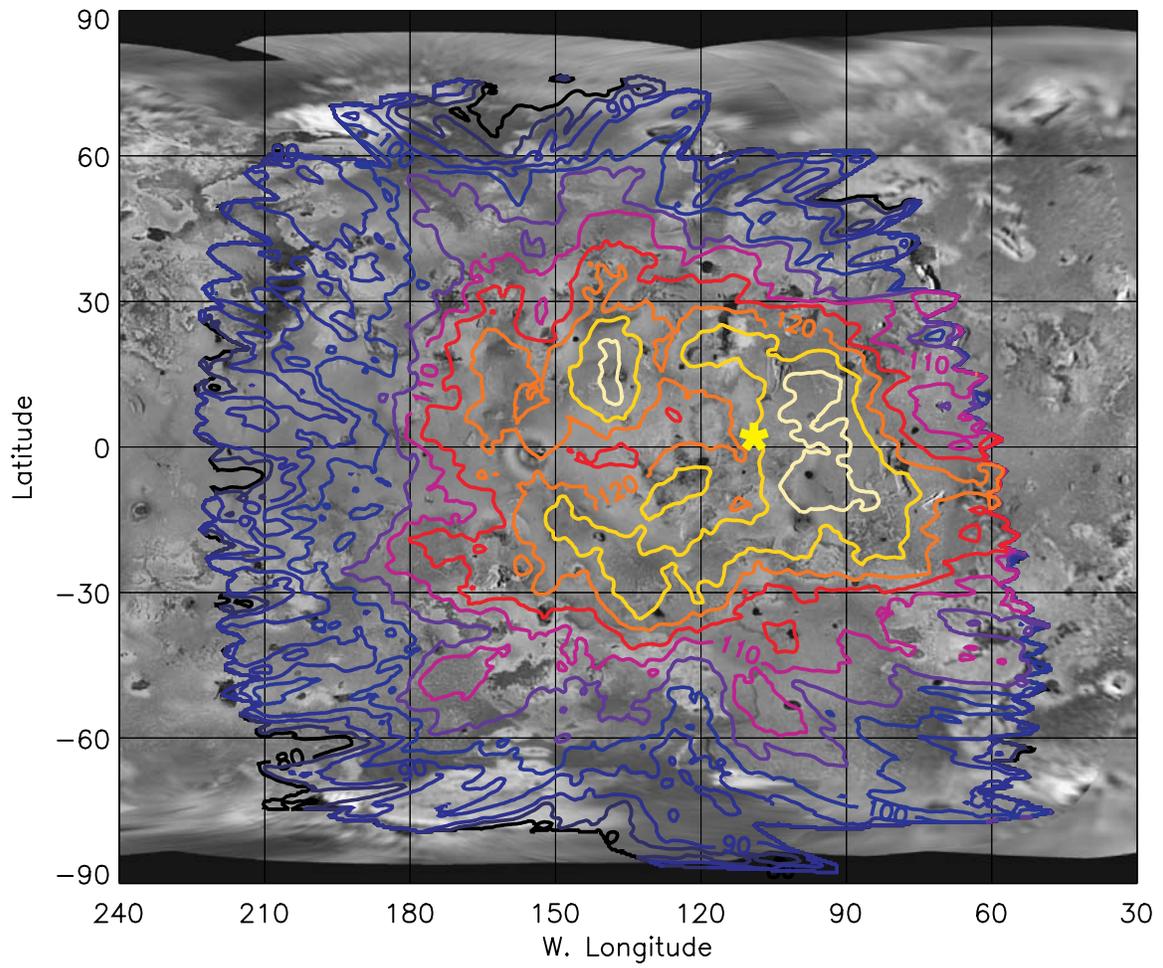
Figure 1 Rathbun et al. Galileo PPR at Io
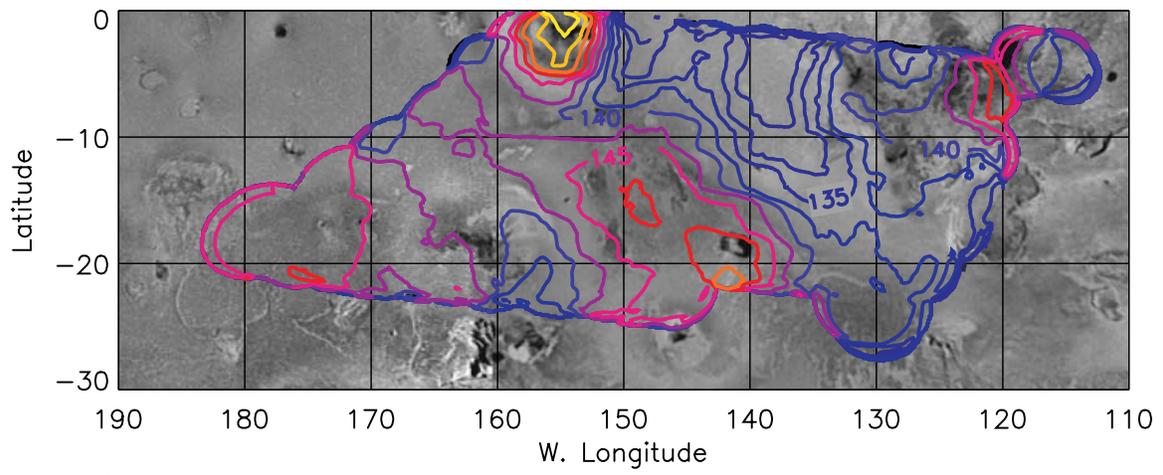
Figure 2 Rathbun et al. Galileo PPR at Io
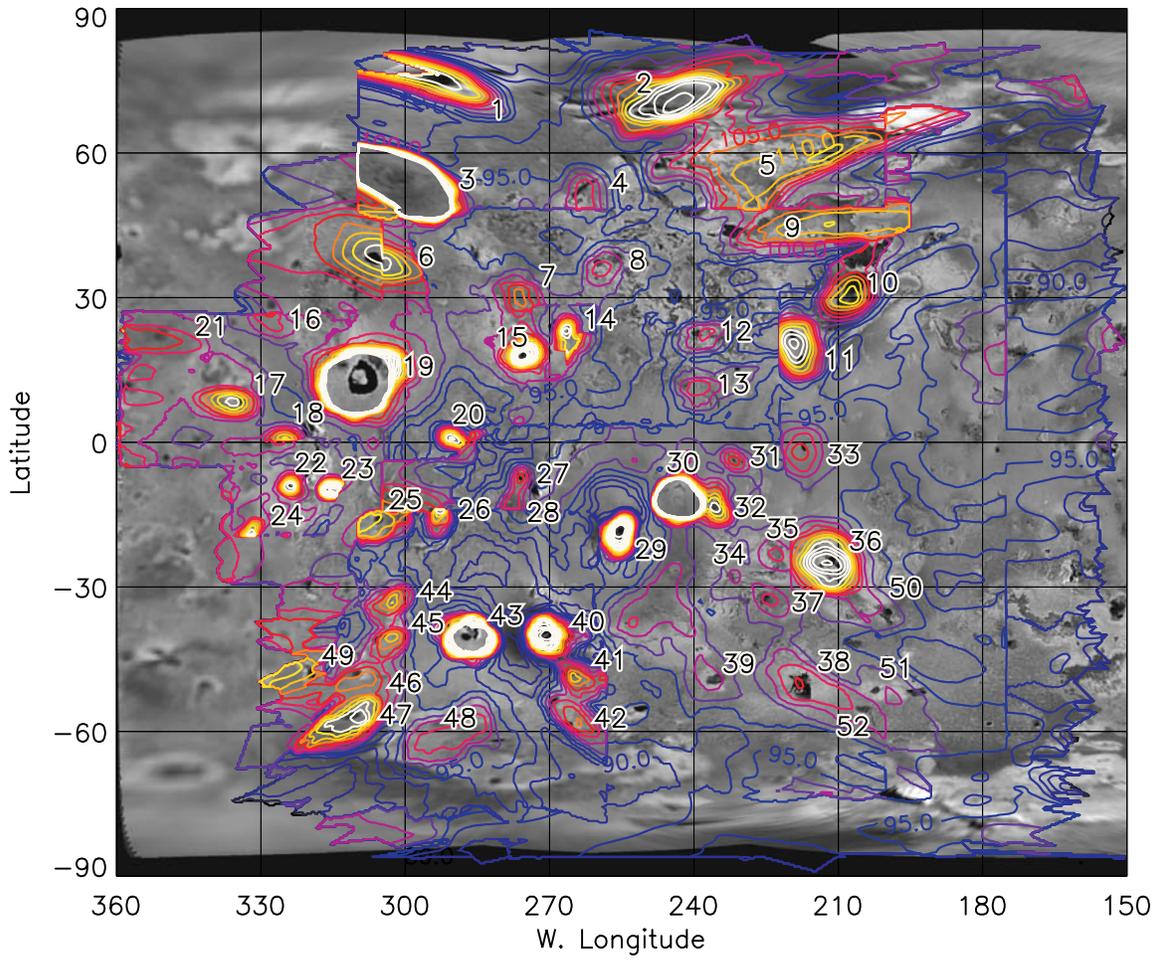
Figure 3 Rathbun et al. Galileo PPR at Io
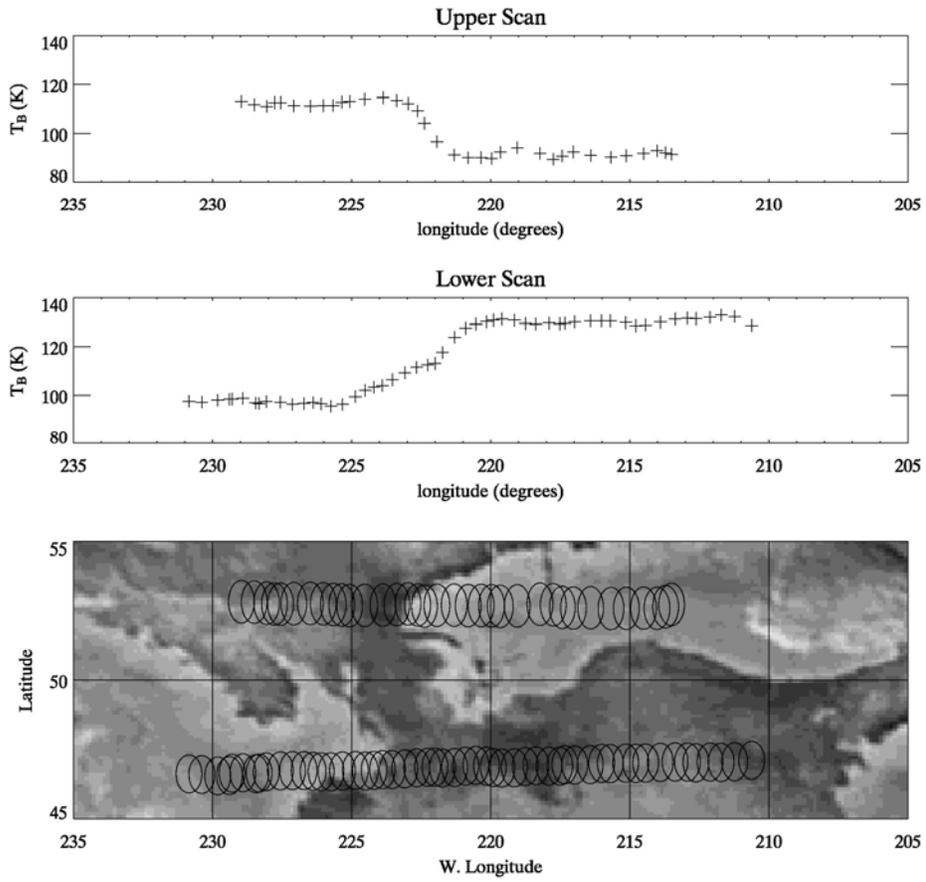
Figure 4 Rathbun et al. Galileo PPR at Io
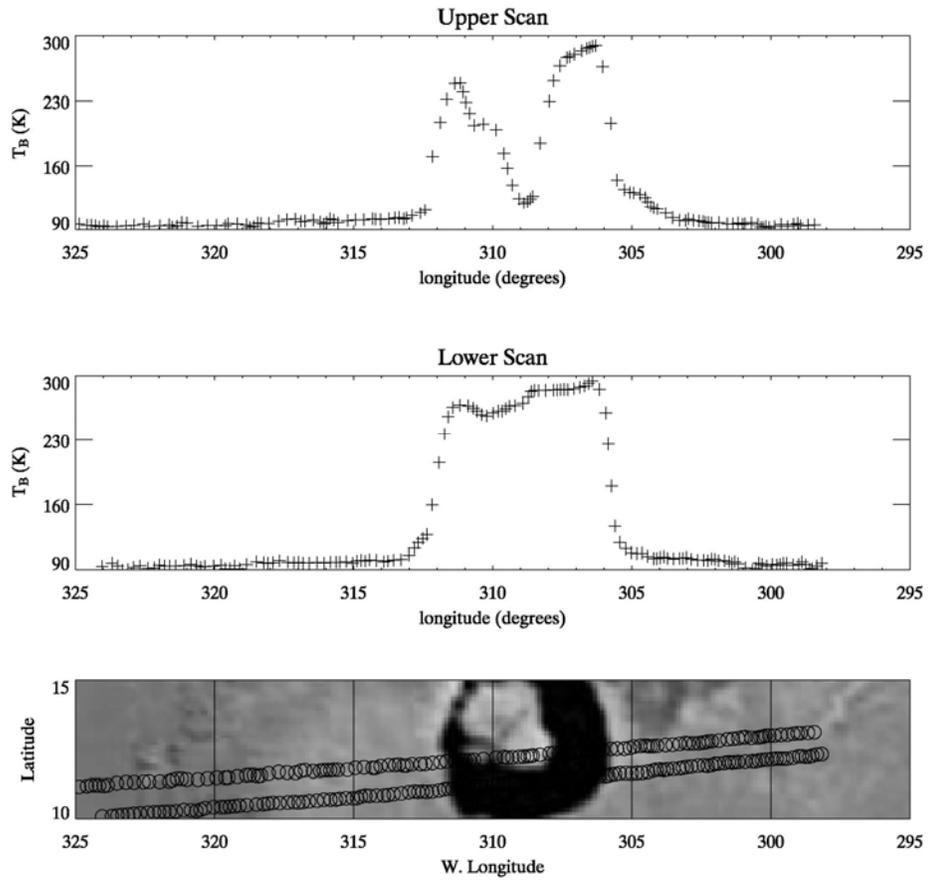
Figure 5 Rathbun et al. Galileo PPR at Io
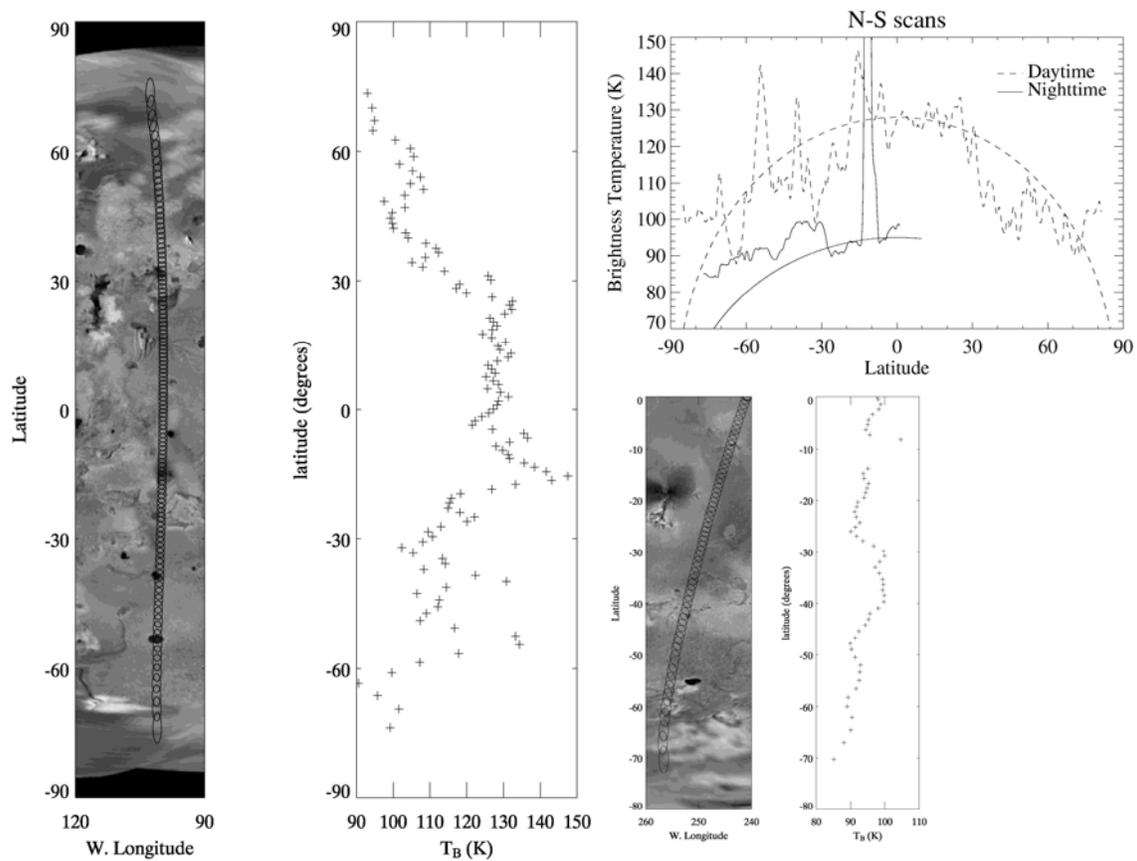
Figure 6 Rathbun et al. Galileo PPR at Io
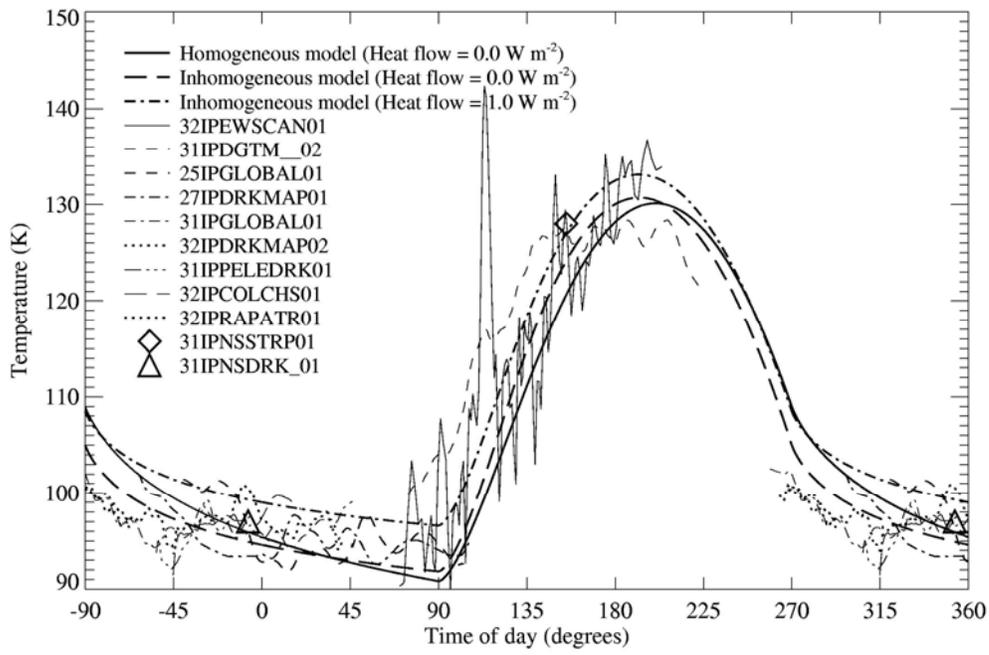
Figure 7 Rathbun et al. Galileo PPR at Io